Studying rogue waves using large-scale direct phase-resolved simulations

Guangyu Wu, Yuming Liu, and Dick K.P. Yue

Department of Mechanical Engineering, // Massachusetts Institute of Technology, Cambridge, Massachusetts 02139

Abstract. We investigate the occurrence and dynamics of rogue waves using large-scale, three-dimensional, phase-resolved simulations. The direct simulations are based on a high-order spectral method. The method resolves the phases of a large number (up to $O(10^7)$) of wave modes, and accounts for nonlinear interactions among them up to an arbitrary high order. Significantly, the simulations obtain exponential convergence, near linear computational effort, and are efficiently implemented on high-performance parallel computers. With this capability we are able to obtain long time (up to $O(10^4)$ sec) nonlinear evolutions of large (up to $O(10^{2\sim3})$ km^2) phase-resolved three-dimensional wave-fields. Our interest is to use these simulations to obtain the frequency and distribution of rogue wave occurrences and the nonlinear wave-wave interaction, in particular modulation instability, mechanisms underlying the generation and evolution of such rogue waves in open seas.

We present the findings from a typical simulation of a nonlinear wave-field generated from JONSWAP spectrum. The occurrence and distribution of rogue waves are analyzed. The local spatial/temporal characteristics of the rogue wave are shown. Energy flux is investigated to explain the formation of rogue waves.

Introduction

The occurrence of rogue waves has been reported by ship crews (*Lavrenov*, 1998; *Lawton*, 2001) and has also been observed in the field wave elevation data (measured at offshore platforms (*Haver*, 2000); and at floating buoys (*Pelinovsky* et al. , 2004) and the satellite ocean surface images (*Dankert* et al. , 2002). Typically, rogue waves have a wave height of two to three times that of the local significant wave height, and a wavelength comparable to the dominant wavelength of the wave-field. Such large steep waves may cause catastrophic damages to offshore structures and surface ships.

Despite a large number of studies, the key mechanisms underling the occurrence and generation of rogue waves remain unclear. In the context of linear wave theories, extreme waves may be formed by a superposition of multiple wave components with an appropriate phase combination (*Brown and Jensen*, 2001). However, the probability of such extreme waves from linear superposition is much smaller than that observed in the field. Moreover, the duration of such extreme waves is much shorter than that of typical rogue waves observed in the field. When wave-current and wave-bottom interactions are considered, wave focusing can result from wave refraction by variable current and bottom topography (*Gerber*, 1993; *Lavrenov*, 1998). While this mechanism might be important in the nearshore area, it does not explain the occurrence of rogue waves observed in deep ocean with weak current. When nonlinear wave effects are accounted for, nonlinear modulation instability (*Janssen*, 2003) and/or nonlinear quartet/quintet resonant wave-wave interactions may play significant roles in the development of rogue waves. Based on the field data measured at nine different locations near Japan, *Yasuda and Mori* (1997) found that the occurrence probability of rogue waves varies with the significant wave height of the wave-field. Nevertheless, the dependence on other physical wave parameters of the wave-field such as frequency distribution and directional spreading were not addressed. Based on a nonlinear Schrodinger equation, *Onorato* et al. (2001, 2002) recently found that for a wave-field given by JONSWAP spectrum, the occurrence of rogue waves increases with the Phillips parameter and the enhancement coefficient, but decreases with the directional spreading. However, this approach is limited to narrowband wave-fields. The effects of (broad) bandwidth and long time nonlinear evolution of the wave-fields on rogue wave formation are still unknown.

In this work, we apply direct large-scale, phase-resolved simulations of three-dimensional nonlinear wave-field evo-

lution to investigate the occurrence and dynamics of rogue waves. The main focus is on the understanding of the effect of nonlinear modulation instability upon the development of rogue waves. Unlike field observations and laboratory experiments which usually obtain either temporal data at a few locations in space or spatial data at a few instants, the present direct simulations provide both temporal and spatial data of a large-scale wave-field. This allows us to study systematically the statistical properties of rogue waves, such as occurrence frequency and spatial/temporal distributions, the local spatial/temporal characteristics and kinematics of rogue waves, and their dependence on physical parameters of the wave-field such as wave height, frequency distribution, and directional spread.

Direct simulations of nonlinear wave-field evolution are obtained using a high-order-spectral (HOS) method (*Dommermuth and Yue*, 1987). The HOS method is developed based on the Zakharov equation and mode-coupling idea. It follows the evolution and resolves the phases of a large number ($O(10^7)$) of wave modes, and accounts for their nonlinear interactions up to an arbitrary high order. In particular, this method achieves an exponential convergence and a (near) linear computational effort with respect to the number of wave modes and the interaction order. Together with these, its high scalability on high-performance computing platforms makes the HOS an effective approach for direct simulations of large-scale nonlinear ocean wave-field evolution.

Specifically, in this study, we simulate the nonlinear evolution of a wave-field generated from JONSWAP spectrum with $\cos^2\theta$ directional spreading. Based on the simulation results, rogue wave events are identified during the evolution of the wave-field, and the local spatial and temporal characteristics of each rogue wave event are analyzed. The focus is on the understanding of the formation mechanism of such events from the viewpoint of energy flux/transfer. Some preliminary results on statistics of rogue waves are also presented.

HOS simulations of three-dimensional nonlinear wave-field evolution

We apply the high-order spectral method to simulate the nonlinear evolution of a large-scale three-dimensional ocean (surface) wave-field in deep water. For simplicity, we assume that there is no wind input. The dissipation due to wave breaking is modeled by a low-pass filter in wavenumber domain (for small scale spilling breaking) and a local smoothing in physical domain (for large scale plunging breaking). In the interest of present study, the nonlinear wave-wave interactions are considered up to the third order (M=3) though the higher order effects can be accounted for without difficulty in HOS simulations. A square computational domain,

28.7km $\times$ 28.7km is used. Doubly periodic boundary conditions in the horizontal directions are employed.

In the simulation, the spatial resolution is $N_X \times N_Y = 4096 \times 4096$ with $\Delta x = \Delta y = 7.0$ m. The waves captured in the simulation are those with wavelengths between 28.0 m and 28.7 km. The wavenumber resolution is $0 \le k_x/\Delta k \le 1024$ and $-1024 \le k_y/\Delta k \le 1024$ with $\Delta k = 0.00022\,\mathrm{m}^{-1}$

To obtain an initial nonlinear wave-field for HOS simulations, we employ a linear wave-field (with random phase for each wave component) as the initial condition and simulate its nonlinear evolution using HOS for a period of time, say T_a. The effect of non-physical phase combination of the initial wave-field is removed by smoothing out breaking waves during this period of evolution. The resulting nonlinear wave-field at $t = T_a$ is then used as the initial condition of HOS simulations for the study of rogue wave development.

In this study, the initial linearized wave-field is given by

$$\eta(x, y, t=0) = \sum_{m=0}^{1024} \sum_{n=-1024}^{1024} \eta_{mn} \,,$$

$$\phi(x, y, t=0) = \sum_{m=0}^{1024} \sum_{n=-1024}^{1024} \phi_{mn} \,,$$

where

$$\eta_{mn} = A_{mn} \cos[m\Delta k\, x + n\Delta k\, y + \alpha_{mn}] \,,$$

$$\phi_{mn} = \frac{gA_{mn}}{\omega_{mn}} \sin[m\Delta k\, x + n\Delta k\, y + \alpha_{mn}].$$

In the above, η represents the free surface elevation and ϕ is the velocity potential on the free surface. And ω_{mn}, A_{mn}, and α_{mn} are respectively the frequency, amplitude and phase of the wave component with wavenumber $(k_{xm}, k_{yn}) = (m\Delta k, n\Delta k)$. The phase α_{mn} is assigned by a random value in $[0, 2\pi]$. The amplitude A_{mn} is obtained from the wavenumber spectrum $S_{\mathbf{k}}(k_x, k_y)$:

$$A_{mn} = [2S_{\mathbf{k}}(m, n)]^{\frac{1}{2}} \Delta k \qquad (1)$$

where $S_{\mathbf{k}}(m, n) \equiv S_{\mathbf{k}}(k_{xm}, k_{yn}) \equiv S_{\mathbf{k}}(m\Delta k, n\Delta k)$. The wavenumber spectrum is related to the frequency-direction spectrum (in deep water) $S(\omega, \theta)$ by:

$$S_{\mathbf{k}}(m, n) = \frac{g^2}{2\omega_{mn}^3} S(\omega_{mn}, \theta_{mn}) \qquad (2)$$

where g is the gravitational acceleration, and θ_{mn} is the propagation direction of the wave component (k_{xm}, k_{yn}).

If the initial linear wave-field is directly used for nonlinear HOS simulations, spurious high-frequency standing waves may be generated since the initial wave-field does not satisfy the nonlinear free-surface boundary conditions. In order to minimize this effect, we follow *Dommermuth* (2000)

to write the kinematic and dynamic boundary conditions on the free-surface $z = \eta(\mathbf{x}, t)$ in the form:

$$\eta_t - \Phi_z = -W(t)\eta_\mathbf{x} \cdot \Phi_\mathbf{x} \ ,$$

and

$$\Phi_t + \eta = -W(t)\frac{1}{2}(\Phi_\mathbf{x} \cdot \Phi_\mathbf{x} + \Phi_z^2) \ .$$

Here $W(t)$ is a smooth function varying from 0 (at $t = 0$) to 1 (for $t \geq T_a$) (*Dommermuth*, 2000). In this study, we use $T_a = 10T_P$ where T_P is the peak period. Note that for the results shown, the time $t = 0$ corresponds to the instant when this transient process ends.

In this study, we consider a JONSWAP spectrum with a $\cos^2\theta$ directional spreading:

$$S(\omega, \theta) = \frac{\alpha g^2}{\omega^5}\exp\left[-\frac{5}{4}(\frac{\omega}{\omega_0})^{-4}\right]\gamma^{\exp\ -\frac{(\omega-\omega_0)^2}{2\sigma^2\omega_0^2}}\ \frac{2}{\pi}\cos^2\theta \ ,$$

for $-\frac{\pi}{2} \leq \theta < \frac{\pi}{2}$. We use the enhancement coefficient γ=1.0, Phillips parameter α=0.0352 (corresponding to a significant wave height H_S=12 m), and ω_0=0.5236 s^{-1} (corresponding to a peak period T_p=12 s and peak wavelength λ_P=224 m). The coefficient $\sigma = 0.07$ for $\omega \leq \omega_0$ and 0.09 for $\omega > \omega_0$. The effective wave steepness of this wave-field is about 0.1.

In the HOS simulation, the time step is Δt=0.375 s ($T_P/\Delta t = 32$), the simulated wavefield evolution time is T_{Sim}=160T_P, and the nonlinear interaction order is $M = 3$. The simulations are performed on IBM SP4 HPC platform with 256 processors used. The computational time of each simulation is about 100 hours.

Data analysis

At each time step, the simulation obtains the wave elevation and velocity potential of the complete wave-field in both physical and spectral spaces. Based on these data, we perform both statistic and deterministic analysis to understand the occurrence and dynamics of rogue waves.

Spectrum evolution

For statistic analysis, we study the spectrum evolution of the nonlinear wave-field. From HOS simulation, we can obtain A_{mn} at each time step by applying Fourier Transform to the elevation data of the wave-field. Therefore the wavenumber spectrum $S_\mathbf{k}(m, n)$ and frequency-direction spectrum $S(\omega_{mn}, \theta_{mn})$ can be obtained using relations (1) and (2) respectively.

Because the discretized data points $(\omega_{mn}, \theta_{mn})$ correspond to a uniform grid in the wavenumber space but not in the frequency-direction space, $S(\omega_{mn}, \theta_{mn})$ cannot be used directly to compute direction-integrated frequency spectrum or frequency-integrated direction spectrum. Thus, we need

to transform the non-uniformly discretized frequency-direction spectrum, $S(\omega_{mn}, \theta_{mn})$, to a uniformly discretized one. For this purpose, we discretize the frequency-direction domain with grids defined by

$$\omega_i = i\Delta\omega, \quad i = 1, ..., N_\omega$$

and

$$\theta_j = -\frac{\pi}{2} + j\Delta\theta, \quad j = 1, ..., N_\theta$$

where N_ω is the number of frequency bands, N_θ is the number of direction bands, $\Delta\omega = \omega_{\text{max}}/N_\omega$, $\Delta\theta = \pi/N_\theta$. Here ω_{max} is the maximum frequency to be analyzed.

The value of the spectrum at each grid (ω_i, θ_j) is then obtained in terms of the non-uniformly-discretized spectrum values around this point:

$$S(\omega_i, \theta_j) = \frac{\sum_{m,n} S(\omega_{mn}, \theta_{mn})R_{ij,mn}}{\sum_{m,n} R_{ij,mn}}.$$

Here the summation is defined to be over all values of m and n satisfying

$$\frac{|\omega_{mn} - \omega_i|}{\Delta\omega} \leq \frac{1}{2} \ \text{ and } \ \frac{|\theta_{mn} - \theta_j|}{\Delta\theta} \leq \frac{1}{2} \ .$$

$R_{ij,mn}$ is the weighting function, which we choose to be the inverse of the distance between $(\omega_{mn}, \theta_{mn})$ and (ω_i, θ_j):

$$R_{ij,mn} = \left[\left(\frac{\omega_{mn} - \omega_i}{\Delta\omega}\right)^2 + \left(\frac{\theta_{mn} - \theta_j}{\Delta\theta}\right)^2\right]^{-1/2}.$$

After $S(\omega_i, \theta_j)$ is obtained, the direction-integrated frequency spectrum or frequency-integrated direction spectrum are computed as:

$$S(\omega_i) = \sum_{j=1}^{N_\theta} S(\omega_i, \theta_j) \ ,$$

$$S(\theta_j) = \sum_{i=1}^{N_\omega} S(\omega_i, \theta_j) \ ,$$

and the normalized direction spreading function is:

$$D(\theta_j, \omega_i) = S(\omega_i, \theta_j)/S(\omega_i) \ .$$

In this paper, we use (N_ω, N_θ)=(140, 90) and $\omega_{\text{max}} = 1.4$ s^{-1} for the spectrum evolution analysis.

Rogue wave identification

To study the occurrence and dynamics of rogue waves, we first need to identify the rogue waves from the wave-field. For this purpose, at any given time, we search the surface elevation data of the nonlinear wave-field and find all local crests or troughs $\mathbf{x_0}$. The meaningful trough or crest (useful
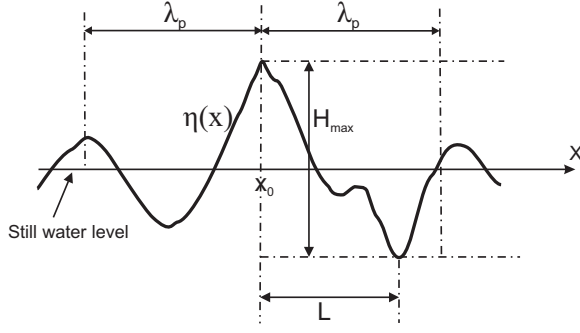
Figure 1. Definition sketch of the local wave height, $H_{\max}$, and the crest-trough distance, L, in an irregular wave-field.

for identifying rogue waves) is defined as the lowest/highest point $\mathbf{x}$ with $|\mathbf{x} - \mathbf{x_0}| \leq \lambda_p$. We define the height between this crest-trough pair to be $H_{\max}$; and the distance between them, L, as shown in Figure 1. The normalized local wave height, α_h, and wave steepness, β are introduced as:

$$\alpha_h \equiv H_{\max}/H_S; \quad \beta \equiv \pi H_{\max}/2L$$

The specific procedure to identify a rogue wave event is:

- For a given rogue wave searching criterion $\alpha_h \geq \alpha_c$, search the wave-field and find all local crests or troughs $\mathbf{x}_j$, which satisfies $|\eta(\mathbf{x}_j)|/H_S \geq \alpha_c/2$;

- For each $\mathbf{x}_j$, find its normalized local wave height α_{hj};

- If $\alpha_{hj} \geq \alpha_c$, $\mathbf{x}_j$ and its corresponding crest or trough form a rogue wave;

- For multiple rogue waves found within a distance of $\lambda_P/2$, only the largest one is followed in this study.

Numerical results

Spectrum evolution

Figure 2 shows the time evolution of the direction-integrated frequency spectrum, $S(\omega)$, of a typical nonlinear wave-field obtained in this study. It is seen that the wave spectrum changes rapidly at the initial stage of evolution and reaches a quasi-steady state after $t/T_P \geq 80$ of evolution. A significant amount of wave energy is lost for waves with frequency larger than the peak frequency during this process while a slight increase of energy for frequency just below the peak frequency is seen. The variation of the spectrum with time for $t > 80T_P$ is much slower than that for $t \leq 80T_P$. Figure 3 plots the variation of the total energy of the wave-field during the evolution. The result indicates that the total energy loss is about 21% (28%) after $80T_P$ ($160\,T_P$) of evolution, compared to the initial wave-field.
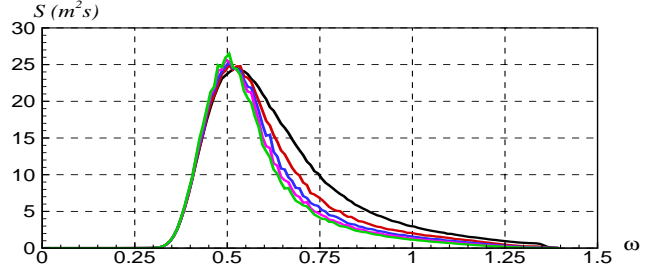

Figure 2. The evolution of direction-integrated frequency spectrum of a nonlinear wave-field. Plotted are the spectrum at time $t/T_P = 0$ (——), 40 (——), 80 (——), 120 (——), and 160 (——).
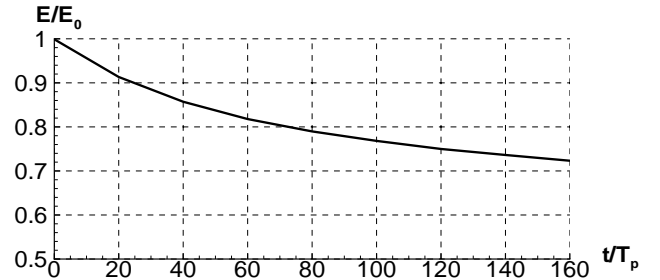

Figure 3. The energy dissipation during nonlinear evolution of the wave-field.
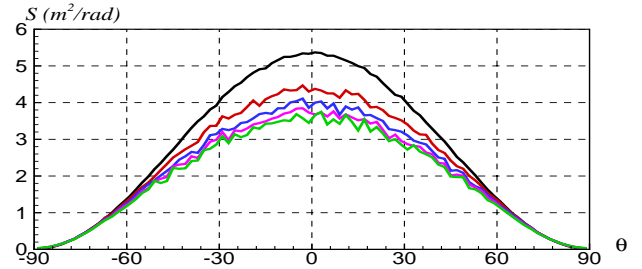

Figure 4. The evolution of frequency-integrated direction spectrum of a nonlinear wave-field. Plotted are the spectrum at time $t/T_P = 0$ (——), 40 (——), 80 (——), 120 (——), and 160 (——).

Figure 4 shows the time evolution of the frequency-integrated direction spectrum, $S(\theta)$. It is similar to that of the frequency spectrum except that a significant amount of energy is dissipated for wave components with direction within $[-60°, 60°]$. To see the dependency of the direction spreading on frequency, we compare the normalized direction spreading function, $D(\theta, \omega)$, at $t/T_P = 0$ and 100. We obtain that at $t = 0$, the direction spreading for all frequency components agrees with the $\cos^2 \theta$ function; while at $t = 100T_P$, the direction spreading deviates significantly from it for $\omega > 1.5\omega_0$. In particular, the direction spreading is broader, and for $\omega > 2\omega_0$, two peaks are formed at $\pm 60°$.
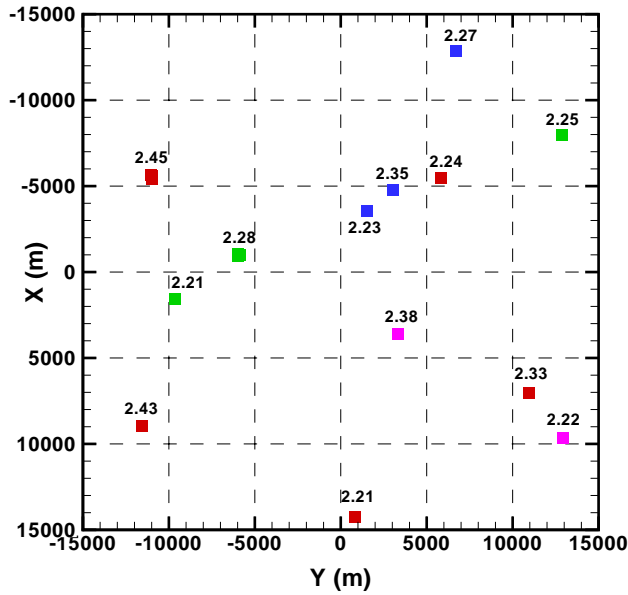
Figure 5. Locations and their corresponding α_h values of rogue waves detected from the simulated wave-field for rogue wave criterion $\alpha_c = 2.2$ at four different instants: t/T_P=100 ( ), 120 ( ), 140 ( ), 160 ( ).

Figure 6. Free-surface elevation contours of the wave-field around a large wave in one rogue wave event at $t/T_P = 98.1$, $\mathbf{x_c} = (8720, -11592)$ m.

Rogue waves

We search the wave-field using a rogue wave criterion of $\alpha_c = 2.2$ at four instants: $t/T_P = 100, 120, 140,$ and 160. The number of rogue wave events detected is respectively 5, 3, 3, and 2. In Figure 5, the spatial distribution of these rogue waves in the simulated ocean wave-field is shown. The rogue waves detected at different instants are marked with colored symbols. It shows that rogue waves can happen anywhere in the wave-field. The local wave height, α_h, of each rogue wave is also shown. The largest rogue wave detected here is α_h=2.45. We also calculate local wave steepness, β, for all these rogue waves. We obtain that 8 (out of 13) rogue waves have β in between 0.2 and 0.3; three have β in between 0.3 and 0.4; and the other two have β in between 0.1 and 0.2.

Evolution of rogue waves

To study the local spatial and temporal characteristics of rogue waves, we focus on one example of the rogue waves. This wave occurs at $t/T_P = 100$, $\mathbf{x}_c = (8970, -11567)$ m with $\alpha_h = 2.43$, where $\mathbf{x}_c$ is the position of the rogue wave crest. By following the evolution of the wavefield around this rogue wave event from t/T_P=95 to 105, we find that the rogue wave event has a group-like behavior, in which three large waves appear subsequently at different locations along the wave propagation direction. The
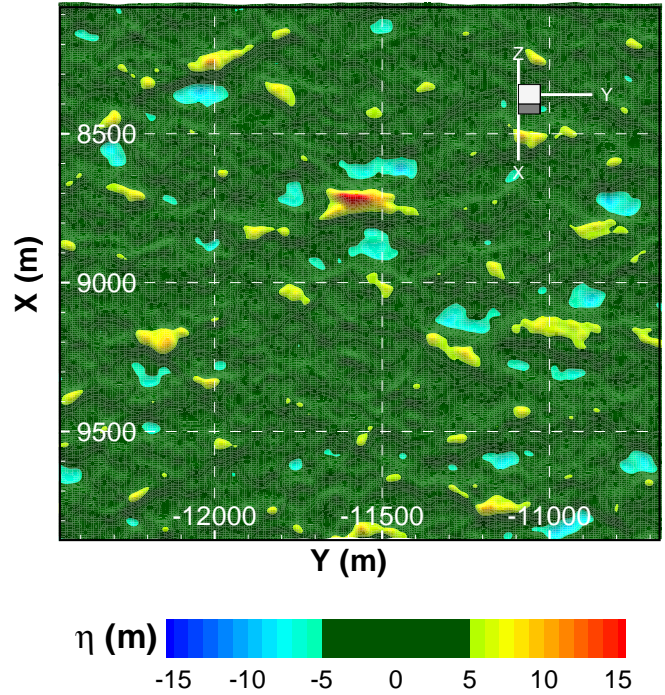
rogue wave detected at t/T_P=100 is actually the third large wave in this group. These three large waves appear in order at t/T_P =96.5, 98.1 and 100; their crests are respectively at $\mathbf{x_c} = (8570, -11567)$ m, $(8720, -11592)$ m and $(8970, -11567)$ m. We see that the y coordinates of these three crests are almost the same, indicating the rogue wave propagates almost in the same direction as that of the dominant wave. Based on the crest location and time of the first and third large waves, the velocity of this rogue wave can be estimated to be $0.51\lambda_P/T_P$, which is very close to the group velocity of the dominant wave component.

Figure 6 shows, as an example, the surface elevation contour of the wavefield around the second large wave, which is also the largest one, with α_h=2.66. Only a small part (~ 1.8 km $\times$ 1.8 km) of the total computational domain is shown. Figure 7 shows the time history of the elevation at the crest location of this wave. It is seen that the local wave height is much larger when the rogue wave passes, compared to other times. The period of this local large wave is almost identical to T_P. It is also observed that the crest and trough of this wave are strongly asymmetric with the distance of the crest from the mean water line almost doubling that of the trough. Figure 8 shows instantaneous wave profiles along the crosscuts of this wave in the x and y directions. The features of large local wave height and strong asymmetry of crest
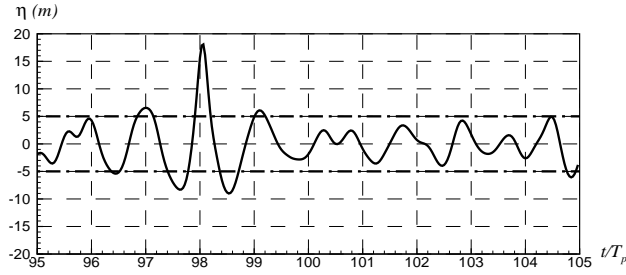
Figure 7. The time history of the free-surface elevation at $\mathbf{x} = (8720, -11592)$ m before and after the rogue wave event.
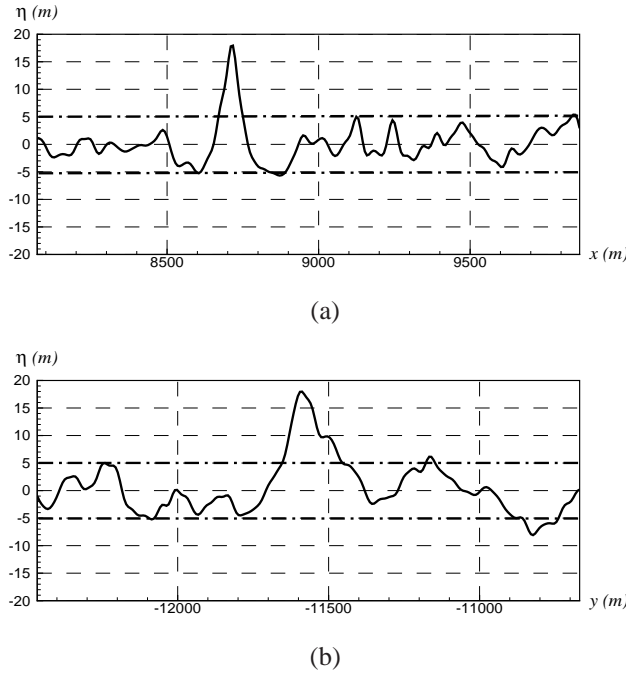

(a)

(b)

Figure 8. Local crosscuts of a large wave in one rogue wave event at $\mathbf{x_c} = (8720, -11592)$ m, $t/T = 98.1$. (a) Crosscut along the x direction at y=-11592 m; (b) Crosscut along the y direction at x=8720 m.

and trough are again observed. The wavelength of the rouge wave in the transverse direction (figure 8b) is about twice that in the longitudinal direction (Figure 8a). This nearly long-crest shape is consistent with the description of rogue waves as "a wall of water" reported in field observation.

Energy flux analysis

To assist the understanding of the mechanism of rogue wave generation, we study the energy density evolution of the wave-field around the rogue wave event shown above. The total energy density at point $\mathbf{x}$ is given by

$$E = E_K + E_P$$

where the potential and kinetic energy densities are respectively given by

$$E_P(\mathbf{x}, t) = \frac{1}{2} g \eta^2(\mathbf{x}, t),$$

and

$$E_K(\mathbf{x}, t) = \int_{-\infty}^{\eta(\mathbf{x}, t)} \frac{1}{2} |\nabla \phi(\mathbf{x}, z, t)|^2 \, \mathrm{d}z \ .$$

We consider a control volume with $x \in [8408, 9075]$ m and $y \in [-11679, -11454]$ m. This is a region with a length of $3\lambda_P$ and a width of λ_P, which includes all three large wave locations in the rogue wave event we discussed above.

The result indicates that the total energy in this control volume starts to increase significantly from $t/T_P = 95$, reaches a maximum value at $t/T_P = 99.2$, and then decreases back to a relatively small value at $t/T_P = 101.5$. This process lasts $6.5T_P$, which is exactly the duration in which the rogue wave develops. This persistence duration, ~ 80 s, is similar to that reported in the field observation. This suggests that energy focusing plays an important role in rogue wave formation.

To understand where the energy in focusing comes from, the energy fluxes across four boundaries of this control volume are calculated as a function of time. The result indicates that the energy focusing and de-focusing during the formation of rogue waves are mainly along the dominant propagation direction of the wave field. This again confirms the locally two-dimensional feature of rogue waves observed in the field.

To further understand the local kinematics of rogue waves, we calculate the growth rate of maximum energy density in the rogue wave group (*Song and Banner* 2002). Although the growth rate obtained is much larger than the threshold value for wave breaking suggested by Song and Banner, the rogue wave in our simulation does not break. The possible reason for this disagreement may be due to the effects of broadband and three-dimensionality of the wave-field. Further investigation on this is underway.

Conclusions

Direct simulations of large-scale three-dimensional non-linear wave-field evolution are employed to investigate the occurrence and dynamics of rogue waves. Sample preliminary simulation results for wave-fields (initially) generated from JONSWAP spectra with $\cos^2 \theta$ directional spreading are presented. A number of rogue wave events are obtained during the nonlinear evolution of the wave-fields. The local temporal and spatial characteristics of a representative rogue wave event is studied in detail. The nearly two-dimensional (long-crested) features of rogue waves are confirmed by examining the wave profiles and the evolution of energy density and energy flux during rogue wave development.

In order to study the dependency of rogue wave statistics on physical parameters, we perform a series of computations using initial wave-fields characterized with varying parameters of the wave-field such as wave height, direction spreading, and frequency distribution of the wave spectrum. In addition to the mechanism associated with modulation instability, we are studying the effects of quartet/quintet resonant wave-wave interactions on rogue wave formation based on longer time evolutions of three-dimensional nonlinear wavefields. The results of these studies will be reported elsewhere.

References

Brown, M.G., and Jensen, A., Experiments on focusing unidirectional water waves, *J. Geophys. Res., 106*, C8, 16917–16928, 2001.

Dankert, H., Horstmann, J., and Rosenthal, W., Detection of extreme waves in SAR images and radar-image sequences, *Proc. 21st Int. Conf. OMAE*, Oslo, Norway, 2002.

Dommermuth, D.G., and Yue, D.K.P., A high-order spectral method for the study of nonlinear gravity waves. *J. Fluid Mech., 184*, 267–288, 1987.

Dommermuth, D.G., The initialization of nonlinear waves using an adjustment scheme, *Wave Motion, 32*, 307–317, 2000.

Gerber, M., The interaction of deep-water gravity waves and an annular current: linear theory, *J. Fluid Mech., 248*, 153–172, 1993.

Haver, S., Evidence of the existence of freak waves, *Proceedings of Rogue Waves 2000, Brest*, 129-140, 2001.

Janssen, P.A.E.M., Nonlinear four-wave interaction and freak waves, *J. Phys. Oceanogr., 33*, 863–884, 2003.

Lavrenov, I.V., The wave energy concentration at the Agulhas Current off South Africa, *Natural Hazards, 17*, 117–127, 1998.

Lawton, G., Monsters of the deep, *New Scientist Magazine, 170*, 2297, 2001.

Onorato, M., Osborne, A.R., Serio, M., and Bertone, S., Freak waves in random oceanic sea states, *Phys. Rev. Lett., 86*, 25, 5831–5834, 2001.

Onorato, M., Osborne, A.R., and Serio, M., Extreme wave events in directional, random oceanic sea states, *Phys. Fluids, 14*, 4, L25–L28, 2002.

Pelinovsky, E., Slunyaev, A., Lopatoukhin, L., Divinsky, B., and Levin, B., Freak wave event in the Black Sea: observation and modelling, *Proceedings of Rogue Waves 2004*, Le Quartz, Brest, France, Oct. 20-22, 2004.

Song, J.-B., and Banner M.L., On determining the onset and strength of breaking for deep water waves. Part I: Unforced irrotational wave groups. *J. Phys. Oceanogr.*, 32, 2541–2558, 2002.

Yasuda, T., and Mori, N., Occurrence properties of giant freak waves in sea area around Japan, *J. Waterway, Port, Coastal, Ocean Eng., 123*, 4, 209–213, 1997.